Nanoscale Fluorescence Imaging of Single Amyloid Fibrils

ARTICLE *in* JOURNAL OF PHYSICAL CHEMISTRY LETTERS · JUNE 2012

Impact Factor: 7.46 · DOI: 10.1021/jz300687f

THE JOURNAL OF PHYSICAL CHEMISTRY Letters

Letter

pubs.acs.org/JPCL

Nanoscale Fluorescence Imaging of Single Amyloid Fibrils

Vijit Dalal,[†,§] Mily Bhattacharya,[‡,§] Dominic Narang,[†] Pushpender K. Sharma,[†] and Samrat Mukhopadhyay*[,†,‡]

[†]Department of Biological Sciences and [‡]Department of Chemical Sciences, Indian Institute of Science Education and Research (IISER), Mohali, Knowledge City, Sector 81, SAS Nagar, Mohali 140306, India

Supporting Information

ABSTRACT: Amyloid formation is implicated in a variety of human diseases. It is important to perform high-resolution optical imaging of individual amyloid fibrils to delineate the structural basis of supramolecular protein assembly. However, amyloid fibrils do not lend themselves to the conventional microscopic resolution, which is hindered by the diffraction limit. Here we show super-resolution fluorescence imaging of fluorescently stained amyloid fibrils derived from disease-associated human β_2-microglobulin using near-field scanning fluorescence microscopy. Using this technique, we were able to resolve the fibrils that were spatially separated by ~75 nm. We have also been able to interrogate individual fibrils in a fibril-by-fibril manner by simultaneously monitoring both nanoscale topography and fluorescence brightness along the length of the fibrils. This method holds promise to detect conformational distributions and heterogeneity that are believed to correlate with the supramolecular packing of misfolded proteins within the fibrils in a diverse conformationally enciphered prion strains and amyloid polymorphs.

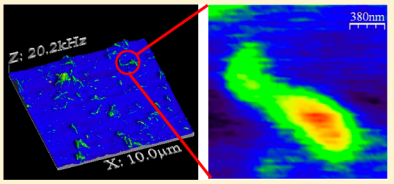

SECTION: Biophysical Chemistry and Biomolecules

Amyloid fibril formation is associated with a number of debilitating human diseases such as Alzheimer's, Parkinson's, Huntington's, and transmissible prion diseases and a number of systemic amyloidosis.[1−8] Recent discoveries have indicated that amyloids may also have beneficial functional roles in a variety of organisms including humans.[9,10] The underlying molecular mechanisms by which amyloids and their precursors are involved in inducing functional consequences, cellular toxicity, and membrane disruption, eventually leading to cell death remain elusive. This is largely due to the fact that conventional optical microscopy does not allow one to monitor these processes directly at a high spatial resolution. The dimensions of amyloid aggregates fall in the nanoscopic regime; therefore, conventional microscopy is inadequate in mapping the supramolecular architecture of the aggregates and their complexes with membrane and other cellular components. High-resolution scanning probe microscopy (SPM)-based imaging technique such as atomic force microscopy (AFM) has been extremely useful in gaining in-depth insight into the nanoscale morphology of various kinds of aggregates and fibrils that could be identified and characterized in various different stages of amyloid assembly.[11−14] However, AFM imaging techniques do not allow us to access the wealth of structural insights that are obtainable from optical microscopy that has been extremely successful in unravelling a wide variety of biological assemblies, interactions, bindings, and colocalizations down to single-molecule resolution. The traditional (far-field) optical microscopy suffers from a major drawback because the far-field (lens-based) focusing creates a focal spot that is fundamentally limited by the optical diffraction-limit (usually ≥250 nm) and poses a bottleneck in the high-resolution imaging to characterize structurally and to localize amyloid fibrils with respect to the cell membrane and other cellular components. Therefore, there is a pressing need to apply and adapt nontraditional optical imaging technologies that will have capabilities in simultaneously mapping fibrils at a high spatial resolution while retaining the wealth of optical (fluorescence) information. One of the ways to perform such high-resolution nanoscale imaging is to utilize SPM-based methods such as near-field scanning optical microscopy (NSOM) that breaks the far-field diffraction limit and allows both topographic and optical mapping simultaneously.[15−25] Near-field imaging using both fluorescence and infrared has been previously applied to many biologically relevant nanoscale systems including protein fibrils.[18−25] Recently, direct stochastic optical reconstruction microscopy (dSTORM) has been applied to achieve a nanoscopic resolution in fluorescence imaging of β-amyloid fibrils.[26]

Here we used human β_2-microglobulin as a model amyloid-forming protein that has been implicated in dialysis-related amyloidosis.[27−29] β_2-microglobulin is a β-rich protein in its native state (Figure 1A) and forms amyloid fibrils under destabilizing conditions such as at low pH.[27−29] The reasons for choosing β_2-microglobulin are as follows: (i) It is an amyloid disease-related protein. (ii) Amyloid fibrils formed in vitro from the recombinantly expressed protein in *Escherichia coli* resemble those found in patients suffering from amyloidosis. (iii) Amyloid formation from this protein is very well characterized by various biophysical tools. (iv) The formation of amyloid

Received: May 28, 2012
Accepted: June 19, 2012

   dx.doi.org/10.1021/jz300687f | *J. Phys. Chem. Lett.* 2012, 3, 1783−1787

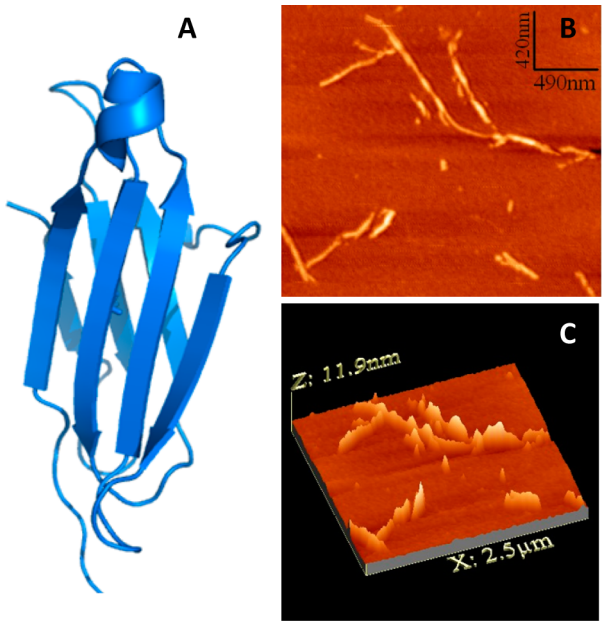

Figure 1. Amyloid fibril formation from human β_2-microglobulin. (A) Crystal structure of human β_2-microglobulin generated using Pymol (Delano Scientific LLC, CA) from protein data bank (PDB ID: 1LDS). (B) AFM image of amyloid fibrils prepared at low pH. (C) 3D AFM topography showing the height profile of fibrils.

fibrils of desired nanoscale morphology is quite reproducible under given conditions.

The AFM image reveals that the fibrils are ~10 nm wide and several hundreds of nanometers long (Figure 1B,C). After characterizing the nanoscale morphology of the fibrils formed under our laboratory conditions, we embarked upon studies aimed at optically imaging these fibrils using fluorescence-mode NSOM. To make the fibrils fluorescent, one can use a fluorescent dye that intercalates in the cross-β structural assembly of amyloid fibrils. Thioflavin-T (ThT) is one such dye that has been used extensively to detect amyloid formation as well as to image the matured fibrils.[30−33] However, ThT suffers from many drawbacks as follows. (i) ThT is charged and can bind nonspecifically to other nonamyloid (amorphous) protein aggregates.[31] (ii) It cannot be used to stain amyloid fibrils that are formed at low pH and disaggregate at neutral pH.[32] (iii) It is not a suitable dye for single-molecule imaging because it has a low fluorescence quantum yield[33] even when bound to amyloid fibrils. (iv) Additionally, this fluorophore cannot be excited using commonly available laser lines such as 488, 532, and 633 nm because it fluoresces at ~482 nm upon binding to amyloid fibrils. To circumvent the aforementioned shortcomings, we used a neutral fluorescent dye, namely, Nile Red that is known to be more specific for amyloid fibrils,[34,35] binds noncovalently to fibrils, and fluoresces over a wide range of pH, demonstrates the sensitivity in nanoscale fluorescence imaging,[36] and can be excited using a commonly available laser line such as 488 nm of Ar^+ laser. (See Figure S1 of the Supporting Information.) After preparing amyloid fibrils from β_2-microglobulin, we have fluorescently stained the fibrils using Nile Red and then deposited them onto freshly cleaved mica that were used for our NSOM studies.

The experimental setup is similar to what has been previously described.[15−23] In our NSOM setup, the 488 nm laser is passed through a metal-coated tapered optical fiber tip having an aperture of ~100 nm (Figure 2A). The fiber is brought close (~10 nm) to the surface of the sample. The light output from

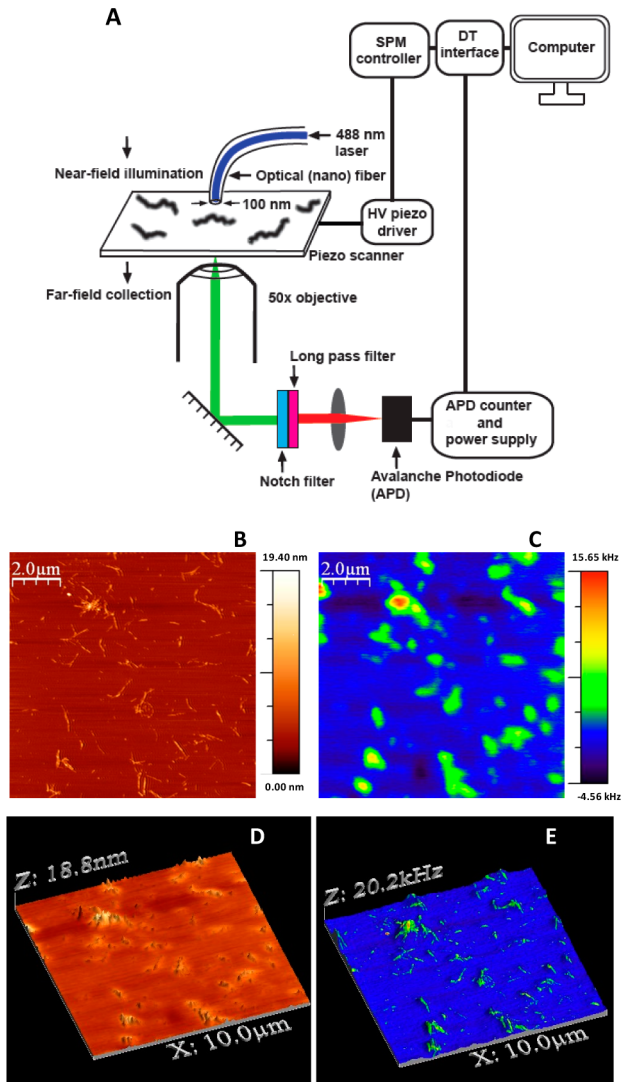

Figure 2. NSOM imaging of β_2-microglobulin amyloid fibrils. (A) Schematic of the experimental set up. (B) Topographic (AFM) and (C) the corresponding fluorescence (NSOM) image of fibrils noncovalently stained with Nile Red. 3D overlays of (D) NSOM fluorescence on AFM topography and (E) AFM topography on NSOM fluorescence, showing they are highly correlated.

the fiber being composed of evanescent waves rather than propagating waves is able to illuminate the "near-field" region that is now limited by the aperture of the fiber but not by the wavelength of the incident light. Therefore, the resolution is substantially higher compared with the diffraction-limit as previously described.[18−23] We have used transmission mode fluorescence NSOM and collected fluorescence emitted from fluorescent fibrils using far-field optics to image the fibrils. The collected fluorescence is passed through a notch filter (488 nm notch) and an appropriate long pass filter (550 LP) and is detected using a highly sensitive avalanche photodiode (APD). The feedback signal is used to generate a topographic map (AFM), and the corresponding fluorescence map is obtained from the emitted photons detected by the APD during scanning.

dx.doi.org/10.1021/jz300687f | J. Phys. Chem. Lett. 2012, 3, 1783−1787

The scanning of the mica surface, containing fluorescent fibrils, using a fiber probe generates topographic as well as fluorescence image simultaneously. Figure 2B shows the AFM topography, whereas Figure 2C shows the corresponding NSOM fluorescence image. These images are highly spatially correlated. This is further illustrated in 3D overlays of both topographic and fluorescence images (Figure 2D,E). Simultaneous line profiling of these images yielded the plots of height (in nanometers) and fluorescence intensity (in kilohertz) along the line drawn against the width of a fibril (Figure 3A). In our

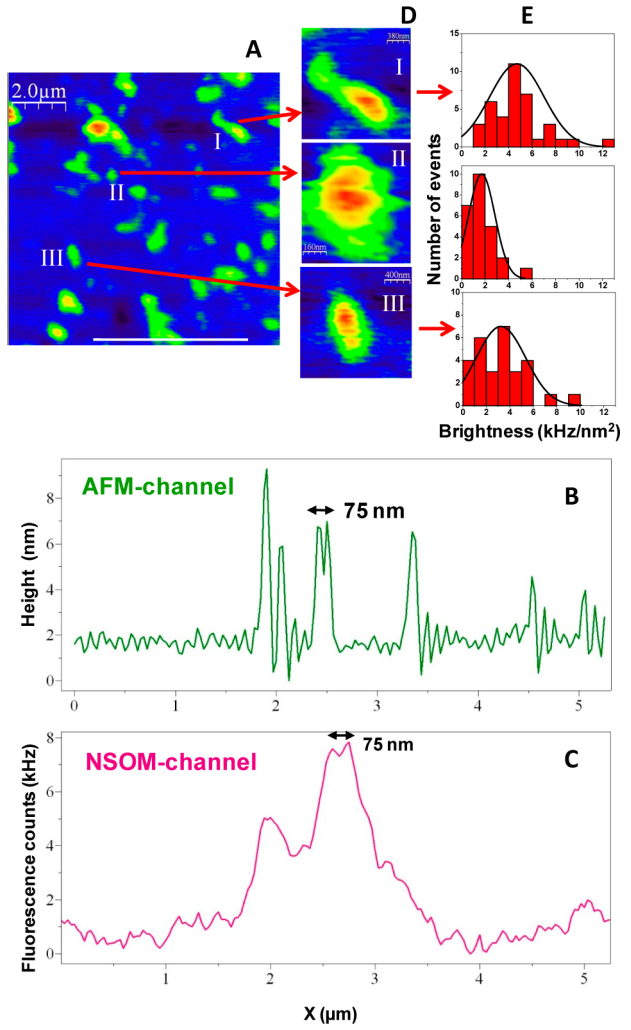

Figure 3. Simultaneous analysis of topography and fluorescence of individual amyloid fibrils obtained from NSOM imaging. (A) NSOM fluorescence image of fibrils showing a few well-separated individual fibrils (I–III). (B) AFM topography and (C) NSOM fluorescence profile along a white line in panel A showing two fibrils that are separated by ~75 nm can be distinguished by NSOM. (D) The zoomed NSOM images and (E) the brightness analysis of the individual fluorescent fibrils indicated I–III. For details of image analysis, see the Experimental Section.

NSOM image, we were able to resolve both the topographic and fluorescence features of two fibrils that are separated by only ~75 nm (shown by double-headed arrows in Figure 3B,C). Our measurements illuminate the fluorescence map of amyloid fibrils at the nanoscopic spatial resolution that is well beyond the diffraction limit and provide a useful handle to visualize and interrogate the supramolecular structural distribution of individual amyloid fibrils using optical information (Figure 3D).

After establishing the spatial correlation between the fibril topography and fluorescence, we next examined whether the fluorescence brightness along the length of an individual fibril is uniform or not. Additionally, we asked whether the observed brightness among different fibrils is uniformly distributed. Our methodology allows us to map out both nanoscopic height profile and fluorescence counts of individual fibrils. Any heterogeneity in the fluorescence brightness is likely to indicate the diversity in structural distribution of these fibrils because the amyloid reporter, Nile Red, may have different binding affinities depending on the supramolecular packing of the cross-β structure within amyloid fibrils. We performed the analysis in the following way. As we have already mentioned that (concurrent) multiple profiling provides both topographic and fluorescence peaks across the width of a fibril, we traversed along the length of the fibril to obtain simultaneous profiles of both height and fluorescence. The area integration of the height profile yielded the cross-sectional area, whereas the integration of the fluorescence profile yielded the total fluorescence counts emitted from the given cross-section of the fibrils. Therefore, the ratio of total fluorescence to the area would yield the fluorescence brightness per unit cross-sectional area (in kHz/nm^2). This analysis was performed for individual fibrils, and the fluorescence brightness per unit area was plotted against the number of events in the form of a histogram (Figure 3D,E). This plot reveals that there is a considerable variation of the brightness along the length of a single fibril indicating a possibility of conformational distribution within the fibril. As previously suggested,[18−20] there might be some contribution from the orientational distributions and the metal (coating of the tip)-induced alterations of both radiative and nonradiative decay rates of fluorophores bound to the fibrils. These effects are likely to contribute to the broadening of the brightness distribution of an individual fibril.

Next, we analyzed the mean brightness and its distribution among different fibrils (Fibrils I–III in Figure 3). This analysis indicated that the mean brightness ranged from 1.7 ± 1.1 to 4.7 ± 2.3 kHz/nm^2 among isolated individual fibrils (Table S1 of the Supporting Information). The brightness distribution for different fibrils in the form of histograms demonstrates considerable variability that is likely to be the result of structural heterogeneity among different individual amyloid fibrils (Figure 3E). We conjecture that the average fluorescence brightness of extrinsic dye, Nile Red, is related to the environment that is felt by the dye around itself in the midst of the supramolecular structure of amyloid fibrils. Because presumably a large number of Nile Red molecules are bound to each of the fibrils and metal-induced alterations in fluorescence are expected to be similar among the fibrils, we believe that the differences in the average brightness among the fibrils are indicative of heterogeneous structural distributions and hence variations in the supramolecular packing of the cross-β architecture. However, we would like to point out that the total area and the total fluorescence have convolutions of the tip used in these measurements. For example, the height profile is typically much sharper compared with the fluorescence profile that is limited by the aperture of the fiber (Figure 3B,C). Therefore, we also performed similar analysis using the ratio of the height and fluorescence peaks (in kHz/nm; the fluorescence maxima in NSOM fluorescence and height maxima in topography) that showed a similar trend with our

dx.doi.org/10.1021/jz300687f | J. Phys. Chem. Lett. 2012, 3, 1783−1787

brightness per unit area analysis (Figure S2 of the Supporting Information). We would like to point out that the maximum fluorescence-to-height ratio ($NSOM_{max}/AFM_{max}$) is devoid of convolutions of the tip because we are considering only the maxima in both height and fluorescence.

In summary, here we have demonstrated nanoscale optical imaging of individual amyloid fibrils using fluorescence. There are several implications of our study presented here. An important achievement involves nanoscopic optical imaging and analysis of single fibrils using Nile Red as an amyloid-sensitive fluorescent reporter that is neutral and works over a wide range of pH and proteins. Additionally, the use of a commonly available laser line broadens significantly the scope of the NSOM methodology and makes amyloid-Nile Red system a very widely viable system for single fibril imaging. Therefore, taken together, this methodology will be applicable for the study of nearly all amyloid systems formed in vitro or isolated from patients. Multiparameter nanoscale structural and optical distribution analysis will be useful to investigate prion strains and amyloid polymorphs that are believed to be enciphered in the protein conformation within the aggregates. We also envision that this methodology coupled to a multicolor illumination and detection format would serve as a powerful tool to probe membrane−amyloid interactions on the cell-surface at the single fibril resolution. Additionally, the analysis combining both topographic and optical information can have incredible potentials in a broad range of surface imaging in biological nanoscopy.

EXPERIMENTAL SECTION

Escherichia coli BL21 (DE3) cells transformed with pET-23a plasmid containing C-terminal His_6-tagged human β_2-microglobulin gene were used for protein expression. The protein was isolated from inclusion bodies and then purified on a Ni-NTA and an anion exchange (Q-sepharose) column. Amyloid fibril formation was carried out in aggregation buffer (20 mM Gly-HCl pH 2.5 containing 200 mM NaCl) with a final protein concentration of 50 μM at room temperature (25 °C) with moderate agitation. For NSOM imaging experiments, an aliquot of Nile Red stock solution in DMSO was added to 10 μL of the mature fibril mixture to a final Nile Red concentration of ∼50 μM, and the sample was incubated for 10 min at 25 °C. (Fluorescence spectra and anisotropy of Nile Red are shown in Figure S1 of the Supporting Information.) Following incubation, the solution was diluted 200-fold with the filtered aggregation buffer, quickly deposited on freshly cleaved mica (Grade V-4 mica from SPI) and allowed to incubate for 15 min. After 15 min, the mica was washed once with 20 μL of filtered aggregation buffer and dried under a gentle stream of ultrapure nitrogen gas for 30 min. During the entire course of sample preparation, utmost care was taken to protect the sample from light to prevent photobleaching. The images were obtained on a MultiView 2000 instrument (Nanonics Imaging, Jerusalem, Israel), operating in the intermittent contact mode and normal-force tuning-fork phase feedback. Online correlated AFM-NSOM images were acquired by Quartz software in a scan area of 10 × 10 μm at a resolution of 320 × 320 pixels with a Z magnification of 1:7 (Z-range 10 μm) under offset sample scanning configuration. During the scans, the sample delay and line delay were kept at 4 and 10 ms, respectively, with the number of substeps as 50. For the method of image analysis, see below.

All of the AFM and online correlated AFM-NSOM images, collected using Quartz software, were imported and processed further using WSxM 4.0 Develop 11.6 image software provided with the instrument.[37] The AFM topography images were processed using parabola flatten and small contrast stretch, following which the respective height profiles were obtained. The AFM-NSOM correlated images, collected simultaneously, were processed using offset flatten and smoothened using Gaussian smooth kernel 2 function. For NSOM images, "extra rain" color palette was used for better visualization. The AFM-NSOM 3D-collages were obtained by overlaying the processed AFM image on the respective NSOM image and vice versa. Further image analysis was carried out for individual fibrils that are well-separated from each other. Simultaneous (multiple) profiling of AFM-NSOM correlated images was employed to obtain the height (from AFM) and fluorescence (from NSOM) profiles from individual fibrils. Multiple line profiling yielded peaks corresponding to both height and fluorescence across the width of an individual fibril. These peaks were integrated to obtain the total cross-sectional area and the total fluorescence along the profile line across the width of the fibril. The brightness per unit area (kHz/nm^2) was estimated from the plots. The mean fluorescence brightness and standard deviations associated with NSOM image analysis of five well-separated individual fibrils are given in Table S1 of the Supporting Information. Several multiple profiling were carried out by traversing along the length of a single fibril. The number of events (or occurrence) for a given fibril was calculated using a binning size of 1 kHz/nm^2 to build the histograms, and this process was repeated for several individual fibrils. Additionally, we calculated the ratio of the fluorescence maxima over the height maxima expressed in kHz/nm. In this case, the binning size was 0.25 kHz/nm to build the histograms (Figure S2 of the Supporting Information). The histograms were plotted using Origin Pro Version 8.

ASSOCIATED CONTENT

Supporting Information

Additional figures on Nile Red binding and NSOM image analysis and a table containing brightness analysis of individual fibrils. This material is available free of charge via the Internet at http://pubs.acs.org.

AUTHOR INFORMATION

Corresponding Author

*E-mail: mukhopadhyay@iisermohali.ac.in.

Author Contributions

§These authors contributed equally to this work.

Notes

The authors declare no competing financial interest.

ACKNOWLEDGMENTS

We thank the members of the Mukhopadhyay lab for critically reading the manuscript, IISER Mohali for providing generous financial support, Dr. H. Taha for assisting us during the measurements, Prof. P. Guptasarma for providing us with the DNA plasmid for β_2-microglobulin and Prof. K. S. Viswanathan for his comments. Research grant from the Council of Scientific & Industrial Research (to S.M.), Women Scientists' grant from the Department of Science & Technology (to M.B.), postdoctoral fellowship from the Department of Biotechnology (to P.K.S), and Junior Research Fellowship from the Council of

Scientific & Industrial Research (to D.N.) are gratefully acknowledged.

REFERENCES

(1) Luheshi, L. M.; Crowther, D. C.; Dobson, C. M. Protein Misfolding and Disease: From the Test Tube to the Organism. *Curr. Opin. Chem. Biol.* **2008**, *12*, 25−31.
(2) Chiti, F.; Dobson, C. M. Protein Misfolding, Functional Amyloid and Human Disease. *Annu. Rev. Biochem.* **2006**, *75*, 333−366.
(3) Jahn, T. R.; Radford, S. E. Folding Versus Aggregation: Polypeptide Conformations on Competing Pathways. *Arch. Biochem. Biophys.* **2008**, *469*, 100−117.
(4) Eichner, T.; Radford, S. E. A Diversity of Assembly Mechanisms of a Generic Amyloid Fold. *Mol. Cell* **2011**, *43*, 8−18.
(5) Tycko, R. Molecular Structure of Amyloid Fibrils: Insights From Solid State NMR. *Q. Rev. Biophys.* **2006**, *39*, 1−55.
(6) Moreno-Gonzalez, I.; Soto, C. Misfolded Protein Aggregates: Mechanisms, Structures and Potential for Disease Transmission. *Semin. Cell Dev. Biol.* **2011**, *22*, 482−487.
(7) Lee, J.; Culyba, E. K.; Powers, E. T.; Kelly, J. W. Amyloid β Forms Fibrils by Nucleated Conformational Conversion of Oligomers. *Nat. Chem. Biol.* **2011**, *7*, 602−609.
(8) Eisenberg, D.; Jucker, M. The Amyloid State of Proteins in Human Diseases. *Cell* **2012**, *148*, 1188−1203.
(9) Shorter, J.; Lindquist, S. Prions as Adaptive Conduits of Memory and Inheritance. *Nat. Rev. Genet.* **2005**, *6*, 435−450.
(10) Fowler, D. M.; Koulov, A. V.; Balch, W. E.; Kelly, J. W. Functional Amyloid − From Bacteria to Humans. *Trends Biochem. Sci.* **2007**, *32*, 217−224.
(11) Ban, T.; Yamaguchi, K.; Goto, Y. Direct Observation of Amyloid Fibril Growth, Propagation, and Adaptation. *Acc. Chem. Res.* **2006**, *39*, 663−670.
(12) Adamcik, J.; Mezzenga, R. Adjustable Twisting Periodic Pitch of Amyloid Fibrils. *Soft Matter* **2011**, *7*, 5437−5443.
(13) Lara, C.; Adamcik, J.; Jordens, S.; Mezzenga, R. General Self-Assembly Mechanism Converting Hydrolyzed Globular Proteins Into Giant Multistranded Amyloid Ribbons. *Biomacromolecules* **2011**, *12*, 1868−1875.
(14) Connelly, L.; Jang, H.; Arce, F. T.; Ramachandran, S.; Kagan, B. L.; Nussinov, R.; Lal, R. Effects of Point Substitutions on the Structure of Toxic Alzheimer's β-Amyloid Channel: Atomic Force Microscopy and Molecular Dynamics Simulations. *Biochemistry* **2012**, *51*, 3031−3038.
(15) Betzig, E.; Trautman, J. K. Near-Field Optics: Microscopy, Spectroscopy, and Surface Modification Beyond the Diffraction Limit. *Science* **1992**, *257*, 189−195.
(16) Betzig, E.; Chichester, R. J. Single Molecules Observed by Near-Field Scanning Optical Microscopy. *Science* **1993**, *262*, 1422−1425.
(17) Trautman, J. K.; Macklin, J. J.; Brus, L. E.; Betzig, E. Near-Field Spectroscopy of Single Molecules at Room Temperature. *Nature* **1994**, *369*, 40−42.
(18) Dunn, R. C.; Allen, E. V.; Joyce, S. A.; Anderson, G. A.; Xie, X. S. Near-Field Fluorescent Imaging of Single Proteins. *Ultramicroscopy* **1995**, *57*, 113−117.
(19) Xie, X. S.; Dunn, R. C. Probing Single Molecule Dynamics. *Science* **1994**, *265*, 361−364.
(20) Xie, X. S. Single-Molecule Spectroscopy and Dynamics at Room Temperature. *Acc. Chem. Res.* **1996**, *29*, 598−606.
(21) Lewis, A.; Taha, H.; Strinkovski, A.; Manevitch, A.; Khatchatouriants, A.; Dekhter, R.; Ammann, E. Near-Field Optics: From Subwavelength Illumination to Nanometric Shadowing. *Nat. Biotechnol.* **2003**, *21*, 1378−1386.
(22) de Lange, F.; Cambi, A.; Huijbens, R.; de Bakker, B.; Rensen, W.; Garcia-Parajo, M.; van Hulst, N.; Figdor, C. G. Cell Biology Beyond the Diffraction Limit: Near-Field Scanning Optical Microscopy. *J. Cell Sci.* **2001**, *114*, 4153−4160.
(23) Hinterdorfer, P.; Garcia-Parajo, F. M.; Dufrêne, Y. F. Single-Molecule Imaging of Cell Surfaces Using Near-Field Nanoscopy. *Acc. Chem. Res.* **2012**, *45*, 327−336.
(24) Kitts, C. C.; Vanden Bout, D. A. Near-Field Scanning Optical Microscopy Measurements of Fluorescent Molecular Probes Binding to Insulin Amyloid Fibrils. *J. Phys. Chem. B.* **2009**, *113*, 12090−12095.
(25) Paulite, M.; Fakhraai, Z.; Li, I. T. S.; Gunari, N.; Tanur, A. E.; Walker, G. C. Imaging Secondary Structure of Individual Amyloid Fibrils of a β_2-Microglobulin Fragment Using Near-Field Infrared Spectroscopy. *J. Am. Chem. Soc.* **2011**, *133*, 7376−7383.
(26) Schierle, G. S. K.; van de Linde, S.; Erdelyi, M.; Esbjörner, E. K.; Klein, T.; Rees, E.; Bertoncini, C. W.; Dobson, C. M.; Sauer, M.; Kaminski, C. F. In Situ Measurements of the Formation and Morphology of Intracellular β-Amyloid Fibrils by Super-Resolution Fluorescence Imaging. *J. Am. Chem. Soc.* **2011**, *133*, 12902−12905.
(27) Gosal, W. S.; Morten, I. J.; Hewitt, E. W.; Smith, D. A.; Thomson, N. H.; Radford, S. E. Competing Pathways Determine Fibril Morphology in the Self Assembly of Beta2-Microglobulin Into Amyloid. *J. Mol. Biol.* **2005**, *351*, 850−864.
(28) Platt, G. W.; Radford, S. E. Glimpses of the Molecular Mechanisms of β_2-Microglobulin Fibril Formation in Vitro: Aggregation on a Complex Energy Landscape. *FEBS Lett.* **2009**, *583*, 2623−2629.
(29) Eichner, T.; Kalverda, A. P.; Thompson, G. S.; Homans, S. W.; Radford, S. E. Conformational Conversion During Amyloid Formation at Atomic Resolution. *Mol. Cell* **2011**, *41*, 161−172.
(30) Levine, H., III. Quantification of β-Sheet Amyloid Fibril Structures With Thioflavin T. *Methods Enzymol.* **1999**, *309*, 274−284.
(31) Nilsson, M. R. Techniques to Study Amyloid Fibril Formation In Vitro. *Methods* **2004**, *34*, 151−160.
(32) Khurana, R.; Coleman, C.; Ionescu-Zanetti, C.; Carter, S. A.; Krishna, V.; Grover, R. K.; Roy, R.; Singh, S. Mechanism of Thioflavin T Binding to Amyloid Fibrils. *J. Struct. Biol.* **2005**, *151*, 229−238.
(33) Sulatskaya, A. L.; Maskevich, A. A.; Kuznetsova, I. M.; Uversky, V. N.; Turoverov, K. K. Fluorescence Quantum Yield of Thioflavin T in Rigid Isotropic Solution and Incorporated Into the Amyloid Fibrils. *PLoS One* **2010**, *5*, e15385.
(34) Mishra, R.; Sörgjerd, K.; Nyström, S.; Nordigården, A.; Yu, Y.-C.; Hammarström, P. Lysozyme Amyloidogenesis is Accelerated by Specific Nicking and Fragmentation but Decelerated by Intact Protein Binding and Conversion. *J. Mol. Biol.* **2007**, *366*, 1029−1044.
(35) Mishra, R.; Sjolander, D.; Hammarström, P. Spectroscopic Characterization of Diverse Amyloid Fibrils In Vitro by the Fluorescent Dye Nile Red. *Mol. Biosyst.* **2011**, *7*, 1232−1240.
(36) Zeisel, D.; Dutoit, B.; Deckert, V.; Roth, T.; Zenobi, R. Optical Spectroscopy and Laser Desorption on a Nanometer Scale. *Anal. Chem.* **1997**, *69*, 749−754.
(37) Horcas, I.; Fernández, R.; Gómez-Rodríguez, J. M.; Colchero, J.; Gómez-Herrero, J.; Baro, A. M. WSxM: A Software for Scanning Probe Microscopy and a Tool for Nanotechnology. *Rev. Sci. Instrum.* **2007**, *78*, 013705−013708.